Advanced Biomedical Engineering
2: 63–71, 2013.

Original Paper

Spin-Lock Imaging for Direct Detection of Oscillating Magnetic Fields with MRI: Simulations and Phantom Studies

Shizue NAGAHARA,[*, **, #] Masahito UENO,[*] Tetsuo KOBAYASHI[*]

Abstract A functional magnetic resonance imaging (fMRI) method that focuses on neural magnetic fields has great potential to detect neural activities more directly than the conventional method. Because this fMRI method does not depend on blood-oxygenation-level-dependent contrast, improved temporal and spatial resolutions can be expected. Among various approaches of this fMRI method, the one that uses a spin-lock imaging sequence has attracted wide attention because of the possibility to detect small oscillating magnetic fields. To understand the mechanism of this approach, we visualized magnetization behavior during the spin-lock module with externally applied oscillating magnetic fields. A fast-and-simple method with matrix operations was used to solve a time-dependent Bloch equation. In addition, we investigated the influence of the duration of the spin-lock pulse in the spin-lock module, which interacts with the external oscillating magnetic fields, on magnetic resonance signals. Furthermore, to detect minute magnetic fields in the order of sub-nT, we carried out phantom studies on the practical use of this method as an fMRI approach. A single-loop coil generating oscillating magnetic fields was placed inside a saline-filled phantom. Time-dependent performance of magnetization during the spin-lock module was thus visually demonstrated to aid understanding of the mechanism of the fMRI method with the spin-lock imaging sequence. In addition to this visualization, we found that the decrease in magnetization depends on the duration of the spin-lock pulse. Longer durations are appropriate for detecting minute sub-nT magnetic fields such as neural magnetic fields. Furthermore, we were able to detect magnetic fields of approximately 200 pT by choosing a spin-lock pulse of long duration and increasing the number of MR image acquisitions. Our results provide useful information for the understanding of the mechanism of direct detection of oscillating neural magnetic fields using MRI with a spin-lock imaging sequence. In addition, we propose an improved selection scheme for the duration of the spin-lock pulse and the feasibility of detecting oscillating magnetic fields of 200 pT considering practical application of fMRI.

Keywords: functional magnetic resonance imaging, Bloch equation, spin-lock imaging sequence.

Adv Biomed Eng. **2**: pp. 63–71, 2013.

1. Introduction

In contrast to electromagnetic measurements of human brain function, such as electroencephalography and magnetoencephalography (MEG), conventional functional magnetic resonance imaging (fMRI) is based on the hemodynamic response occurring after brain activation rather than the neuronal activation itself. Magnetic resonance (MR) signal changes originating from this hemodynamic change constitute the blood-oxygenation-level-dependent (BOLD) effect [1], which limits spatial and temporal resolutions and does not clarify the correlation between brain activation and the BOLD effect [2–4]. However, despite its indirect approach, BOLD fMRI is a powerful tool for noninvasive brain function mapping. Therefore, to maximize its advantages — ease of measurement and relatively high resolutions — the development of a new fMRI method has attracted considerable research effort.

In recent years, development of new fMRI methods that allow direct detection of neural magnetic fields has been anticipated [5–11]. Although successful detection of magnetic fields in fMRI experiments has not been documented, some researchers claim that such fields are observable with MRI scanners [6, 8, 10, 11]. Researchers have attempted to detect changes in phase or magnitude of the magnetization generated by subtle and transient alternations of static magnetic fields (B_0) resulting from neural activity. However, these changes are weak and may be difficult to detect. In addition, phase cancellation induced by incoherent neuron orientation may influence the results obtained using this method [5, 7].

A new fMRI approach to detect neural magnetic fields was reported by Witzel et al. [12] in 2008. They proposed that the intensity of MR signals decreases due to interactions between a pulse in the spin-lock sequence and externally applied magnetic fields oscillating at its

Received on July 10, 2013; revised on September 24, 2013; accepted on October 10, 2013.

[*] Department of Electrical Engineering, Graduate School of Engineering, Kyoto University, Kyoto, Japan.

[**] Research Fellow of the Japan Society for the Promotion of Science.

[#] A1–216, Kyotodaigaku-katsura, Nishikyo-ku, Kyoto 615–8510, Japan.
E-mail: nagahara@bfe.kuee.kyoto-u.ac.jp

resonant frequency. This phenomenon is called stimulus-induced rotary saturation (SIRS), and has been demonstrated by simulations and phantom studies. Witzel et al. [12] used a dipole phantom and detected magnetic fields of 1 nT at 1.5 mm from the dipole. Furthermore, Halpern-Manners et al. [13] reported fundamental studies on this fMRI approach. They used a phantom with a loop wire and mapped its magnetic field to achieve the desired detection sensitivity. In this approach using SIRS, magnetic field detection is not related to the observation of changes in phase or magnitude of magnetization. Therefore, many issues related to the cancellation of accumulated phase can be ignored. Moreover, it has the advantage of being able to detect oscillating magnetic fields such as α (8–13 Hz) and γ (25–150 Hz, including high-γ) waves [14] because there is no limitation on imaging oscillating magnetic fields with frequencies above～10 Hz [13, 15]. Aside from this fMRI approach, Jin and Kim [16] reported a non-hemodynamic fMRI approach using spin-lock imaging. They focused on a small tissue-originated $T_{1\rho}$ change, which is measured by MRI using a spin-lock imaging sequence. This result is inconsistent with fMRI studies [12, 13] using spin-lock imaging based on detection of neural magnetic fields. Therefore, the mechanism of fMRI using spin-lock imaging is still controversial. However, we propose that direct detection of magnetic fields warrants further study to prove the possibility of detecting neural magnetic fields by MRI.

One of the goals of our study was to visualize magnetization performance when magnetic resonance occurs between a pulse of the spin-lock imaging sequence, called the spin-lock pulse, and externally applied magnetic fields oscillating at its resonant frequency, a phenomenon referred to as SIRS. Here, we define this interaction as the secondary magnetic resonance that occurs after the initial magnetic resonance between the static magnetic field B_0 and the radio frequency (RF) excitation pulse. We solved the Bloch equation [17] numerically for this visualization and employed a doubly rotating frame to solve the Bloch equation [12]. This visualization should improve the understanding of how spin-lock imaging may permit magnetic field detection for further investigation. We confirmed this phenomenon through simulations and phantom studies with a single-loop coil while attempting to achieve the other goal of our study, which was the detection of sub-nT magnetic fields. In the simulations, we observed the secondary magnetic resonance as well as investigated the dependence of magnetization (intensity of MR signal) decreases on the duration of the spin-lock pulse. Based on this simulation, sub-nT magnetic fields were detected in the phantom study.

2. Theory

Spin-lock imaging has been used in biomedical imaging [18]. The spin-lock sequence includes a spin-lock pulse, which is a long-duration, low-power pulse, and is used to lock the spins in the transverse plane [19]. It provides images based on $T_{1\rho}$ relaxation, which is the spin-lattice relaxation time in the rotating frame [18].

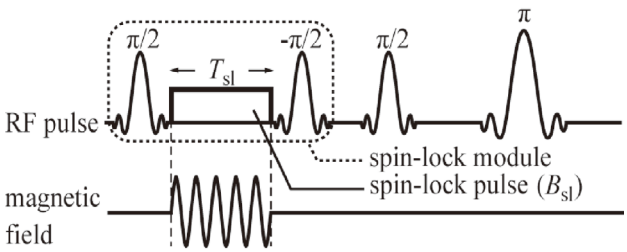

Fig. 1 Spin-lock imaging sequence comprising the spin-lock module, which consists of two $\pi/2$ pulses with a spin-lock pulse in between, and a conventional spin-echo sequence. B_{sl} and T_{sl} are the amplitude and duration, respectively, of the spin-lock pulse.

Figure 1 shows a spin-lock imaging sequence consisting of two parts: a spin-lock module and a spin-echo sequence. The spin-lock module comprises two $\pi/2$ pulses and a spin-lock pulse (with amplitude B_{sl} and pulse duration T_{sl}) in between. The conventional spin-echo sequence is used to obtain MR images.

As shown in **Fig. 2a**, the first $\pi/2$ pulse is applied parallel to the x'-axis in the rotating frame. This flips the initial magnetization **M** (M_x, M_y, M_z), which is aligned along the direction of the static magnetic field $\mathbf{B}_0$ (0, 0, B_0) on the z-axis, to the transverse plane (x-y plane). Then, if the spin-lock pulse, which is the RF pulse oscillating at ω_0, is applied parallel to the y'-axis, it can be expressed as magnetic field $\mathbf{B}_{sl}$ (B_{sl} sin $\omega_0 t$, B_{sl} cos $\omega_0 t$, 0), where $\omega_0 = \gamma B_0$, and γ denotes the gyromagnetic ratio. With the frame rotating at ω_0, B_{sl} acts as a secondary B_0 field (**Fig. 2b**), and locks the flipped **M** in the transverse plane (x-y plane) from the viewpoint of the laboratory frame and in the y'-axis from the viewpoint of the rotating frame. If there are no magnetic fields, or if there is a magnetic field oscillating at an off-resonant frequency of B_{sl} ($\omega_{sl} = \gamma B_{sl}$), magnetic resonance does not occur (**Fig. 2c**). In contrast, a magnetic field oscillating at an on-resonant frequency of B_{sl} flips the direction of **M** (**Fig. 2e**). After time T_{sl}, the second $\pi/2$ pulse is applied and restores M_y along the z-axis. **Figure 2d** shows that the oscillating magnetic field does not affect **M**, whereas **Fig. 2f** shows that oscillating magnetic fields decrease the magnitude of the final **M**. To understand the behavior of **M**, we relabeled the axes of the rotating frame (x', y', z') as follows: x' to y', y' to z', and z' to x'. By these changes, we regard B_{sl} as the secondary B_0 and its direction is considered to be parallel to the z'-axis. Furthermore, after relabeling the axes, we introduced a doubly rotating frame rotating at the same frequency ω as the oscillating magnetic field applied parallel to the x'-axis. Since the oscillating magnetic field acts like an excitation pulse for **M**" locked by the spin-lock field in the doubly rotating frame, the Bloch equation for magnetization behavior in the doubly rotating frame during the spin-lock pulse can be constructed:

$$\frac{dM''_x}{dt} = -\frac{M''_x}{T_2^*} + (\omega_{sl} - \omega) M''_y$$

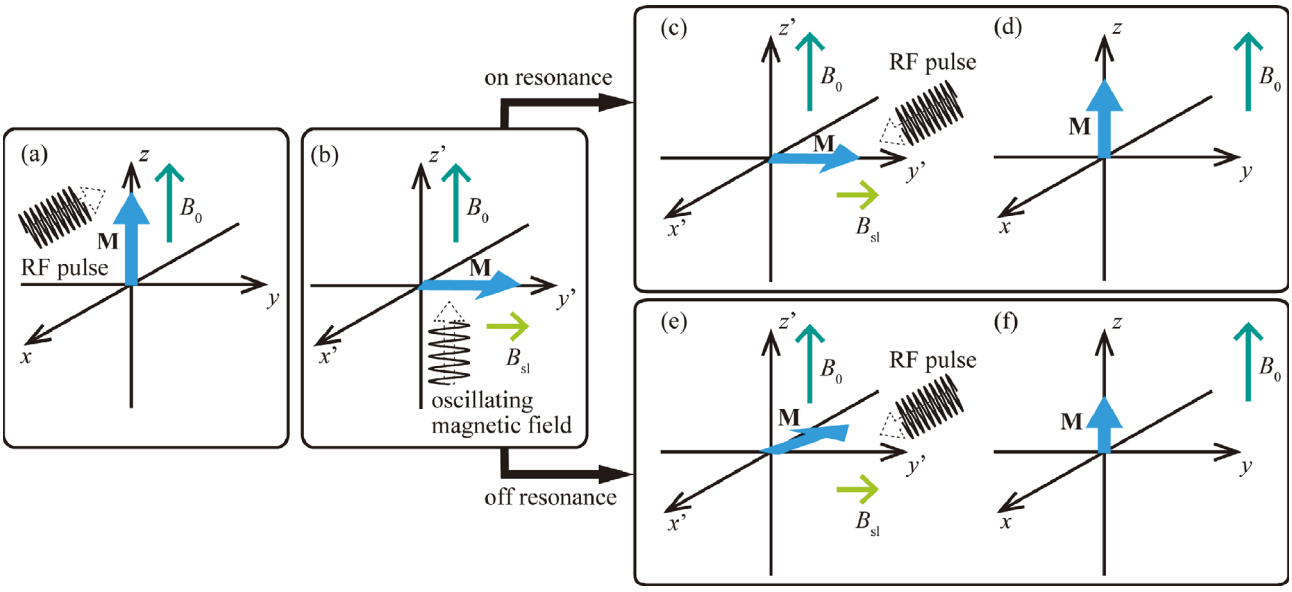

Fig. 2 Externally applied oscillating magnetic fields decrease M_z due to secondary magnetic resonance. (x, y, z) and (x', y', z') are the coordinates of laboratory frame and singly rotating frame, respectively.

$$\frac{dM''_y}{dt} = -(\omega_{sl}-\omega)M''_x - \frac{M''_y}{T_2^*} + \omega_m M''_z \qquad (1)$$
$$\frac{dM''_z}{dt} = -\omega_m M''_y - \frac{M''_z - M''_0}{T_{1\rho}}$$

where $\omega_m = \gamma B_m$. Here, B_m and ω denote the amplitude and frequency, respectively of the oscillating magnetic field. $T_{1\rho}$ and T_2^* denote the $T_{1\rho}$ and T_2^* relaxation time, respectively. Following the application of the spin-lock module, the subsequent spin-echo sequence generates MR signals.

When using this spin-echo sequence with the spin-lock module, an externally applied magnetic field oscillating at the on-resonant frequency of B_{sl} decreases the intensities of MR signals due to the secondary magnetic resonance with the spin-lock field. Based on this effect, by focusing on neural magnetic fields oscillating at specific frequencies such as α and γ waves, it is possible to conduct fMRI studies with spin-lock imaging[12, 13].

3. Methods

Simulation studies based on the Bloch equation were implemented to visualize the behavior of magnetization with the spin-lock module in the spin-lock imaging sequence. In the simulation, we also observed the secondary magnetic resonance of the spin-lock pulse and how the oscillating magnetic fields decrease the magnetization. In addition, the effects of the secondary magnetic resonance on the intensity of MR signals were investigated through phantom studies.

3.1 Simulation based on Bloch equation

First, magnetization behavior in the doubly rotating frame during the spin-lock pulse was calculated by means of a matrix operation[17]. Then, M''_x, M''_y, and M''_z in Eq. 1 were transformed into a singly rotating frame and associated with the magnetization behavior during the $\pi/2$ pulses. Finally, the singly rotating frame components were transformed into the laboratory frame to derive the time-dependent magnetization behavior. In this visualization, we used the following parameters: T_1 = 1100 ms, T_2^* = 75 ms, $T_{1\rho}$ = 100 ms, B_{sl} = 2.35 μT (ω_{sl} = 100 Hz), T_{sl} = 40 ms, B_m = 0/50 nT, and ω = 0/100 Hz. In addition, B_0 was set to 1.5×10^{-5} T to visualize the magnetization behavior clearly.

Next, to observe the secondary magnetic resonance by Bloch simulation, we obtained the magnetization behavior when applying the spin-lock module by fixing the amplitude of the spin-lock pulse B_{sl} at 1.17 and 2.35 μT, while changing the frequency ω of the oscillating magnetic fields. The Larmor frequencies ω_{sl} corresponding to these fixed amplitudes were 50 and 100 Hz, respectively, and T_1, T_2^*, and $T_{1\rho}$ were set to 1100, 75, and 100 ms, respectively, to model human brain gray matter scanned with a 1.5 T MRI[20, 21]. To obtain ω_m, we set B_m at 47 nT, and fixed T_{sl} at 100 ms.

Bloch simulations were also used to investigate a parameter of the spin-lock pulse — the influence of T_{sl} — on the decrease in magnetization during secondary magnetic resonance. With T_1, T_2^*, and $T_{1\rho}$ set at values used in the abovementioned simulations, we increased T_{sl} from 0 to 500 ms while changing B_m to 0.5, 1.0, and 5.0 nT (small values similar to neural magnetic fields). To simulate the secondary magnetic resonance, we set B_{sl} and ω to 2.35 μT (ω_{sl} = 100 Hz) and 100 Hz, respectively.

3.2 Phantom study

To verify our simulations, we observed the signal decrease caused by the secondary magnetic resonance. The phantom consisted of a single-loop coil made of insulated copper wire 0.5 mm in diameter and a cylindrical plastic tube, as shown in **Fig. 3**. The tube was filled with

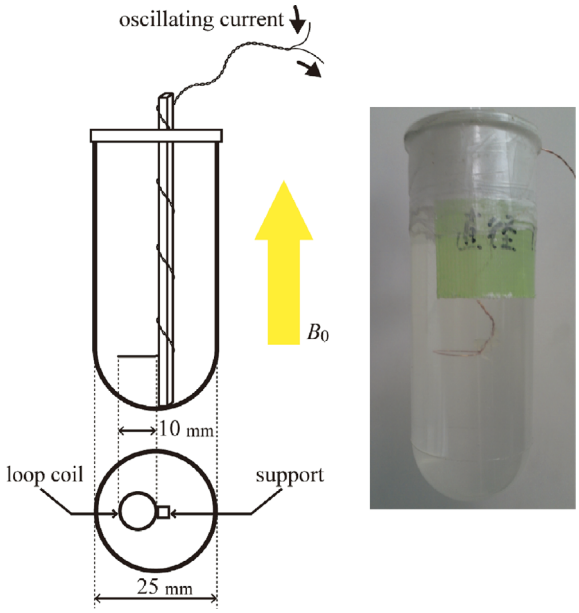

Fig. 3 Phantom consisting of a single-loop coil. The loop is made of insulated copper wire 0.5 mm in diameter and is positioned in a plastic tube filled with saline solution. The wire is twisted to cancel the magnetic fields generated by the wire, except for the loop.

saline (0.9% NaCl) mixed with 0.25 ml of gadopentetate dimeglumine (Magnevist, Berlex Laboratories), yielding T_1 = 1100 ms measured by inversion recovery. The diameter of the loop was 10 mm, and was positioned perpendicular to the B_0 field. The loop was connected to a function generator (AFG3000, Tektronix), which uses a gating pulse controlled by the MR pulse sequence to apply magnetic fields only during the spin-lock pulse of the sequence. In addition, a 2-kΩ resistor was inserted into the circuit. The wire was twisted to cancel the magnetic fields generated by the wire, except for the loop.

Spin-lock imaging was implemented with a 7 T MR scanner (Bruker, BioSpin). We selected this scanner for the phantom study because it allowed us to rewrite the pulse sequence easily and to obtain a high-signal-to-noise ratio. A standard spin-echo sequence was used in this experiment, which is shown in **Fig. 1** as the sequence following the spin-lock module. The T_{sl} was set at 100 ms, and B_{sl} was set at 1.17 and 2.35 μT (ω_{sl} = 50 and 100 Hz). During the spin-lock pulse, the function generator produced an alternating current to generate magnetic fields around the loop. The amplitude of the current was set to 750 μA, generating B_m of 47 nT at the center of the loop. To observe the signal decrease when the secondary magnetic resonance occurs, ω was set to 0–100 and 50–150 Hz, while ω_{sl} was set to 50 and 100 Hz, respectively. Images were acquired with a matrix of 64 × 64, a field of view (FOV) of 4.0 × 4.0 cm, and a slice thickness of 2 mm. Additional parameters included echo time (TE) of 14 ms and repetition time (TR) of 1 s.

A further phantom study was carried out to determine small magnetic fields in the order of sub-nT using this method. The frequency of targeted magnetic field was adjusted to obtain maximum signal decrease. Three amplitudes were selected; 314, 157, and 31.4 pT, at the center of the loop, considering the actual magnetic fields in the human brain [6, 9, 12, 13]. Regarding the spin-lock pulse, T_{sl} and B_{sl} were fixed at 200 ms and 2.35 μT, respectively. Other imaging parameters were set at the same values as those used in the abovementioned phantom study.

4. Results

4.1 Simulation for the Bloch equation

Figure 4 shows the magnetization behaviors during the spin-lock module with an externally applied magnetic field oscillating at off- or on-resonant frequency (B_{sl}). In the case of off-resonant, magnetization (M_x, M_y, M_z) commenced at (0, 0, 1) and was then flipped to the x-y plane (**Fig. 4a**). After being locked in the x-y plane, magnetization returned to the z-axis. The final decrease in M_z was caused solely by $T_{1\rho}$ relaxation (**Fig. 4a-3**). In contrast, in the case of on-resonant, magnetization oscillated three-dimensionally (**Fig. 4b**), because the magnetic field oscillating at the Larmor frequency of the spin-lock pulse flipped it to the plane perpendicular to the spin-lock direction, behaving like an excitation pulse in the doubly rotating frame. Consequently, M_z finally decreased to a greater extent than that in the case of off-resonant.

Figure 5 shows the time courses of M_z using the spin-lock pulse, with amplitudes set to provide ω_{sl} of 100, 95, and 50 Hz. In every case, ω was set to the same value as ω_{sl} to satisfy the on-resonant condition. Although the cycle of each M_z differed, M_z had the same value at the end of the spin-lock module. These results suggest that the decrease in M_z caused by the secondary magnetic resonance is independent of the on-resonant frequencies of the spin-lock pulse and oscillating magnetic fields.

Figure 6 shows that the normalized magnetization M_z (on)/M_z (off) decreased when the applied magnetic field B_m was oscillating at a Larmor frequency of B_{sl}. Here, M_z (on) and M_z (off) are the z component of the magnetization in the presence and absence, respectively, of externally applied on-resonant oscillating magnetic fields. A decrease in the normalized magnetization caused by secondary magnetization was observed with both frequencies: ω_{sl} = 50 and 100 Hz.

The influence of T_{sl} on the decrease of magnetization during secondary magnetic resonance was observed (**Fig. 7**). M_z (on)/M_z (off) were the same as those shown in **Fig. 6**. M_z (on)/M_z (off) decreased to a greater extent with longer T_{sl}.

4.2 Phantom study

As **Fig. 8** shows, the normalized signal intensities S (on)/S (off) decreased when the applied magnetic field oscillated at ω_{sl} (solid lines), similar to the simulation results. Here, S (on) and S (off) are signal intensities in the presence and absence, respectively, of externally applied on-resonant oscillating magnetic fields. The data are average signal intensities of 5 × 5 pixels at the center of the loop coil in the MR images. Together with the

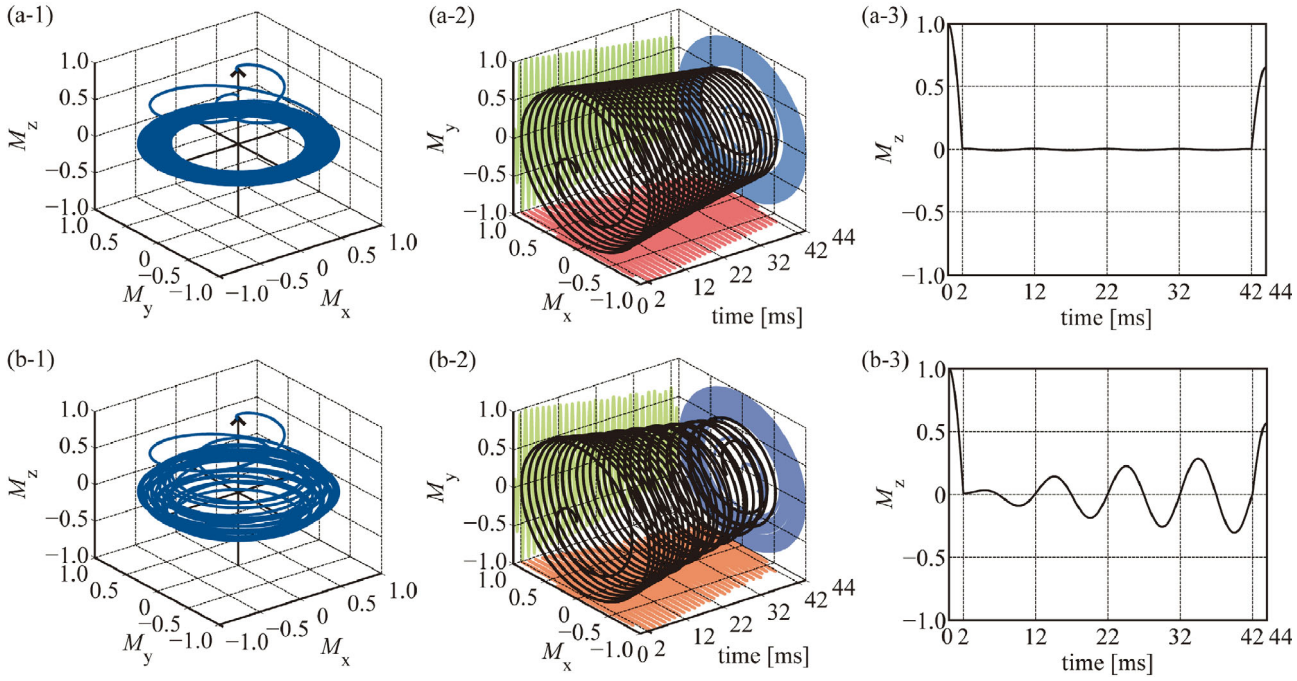

Fig. 4 Magnetization behavior during spin-lock module with an off-resonant oscillating magnetic field applied (a-1), showing time courses of M_x and M_y (a-2) and time course of M_z (a-3). Magnetization behavior during spin-lock module with an on-resonant oscillating magnetic field applied (b-1), showing time course of M_x and M_y (b-2) and time course of M_z (b-3).

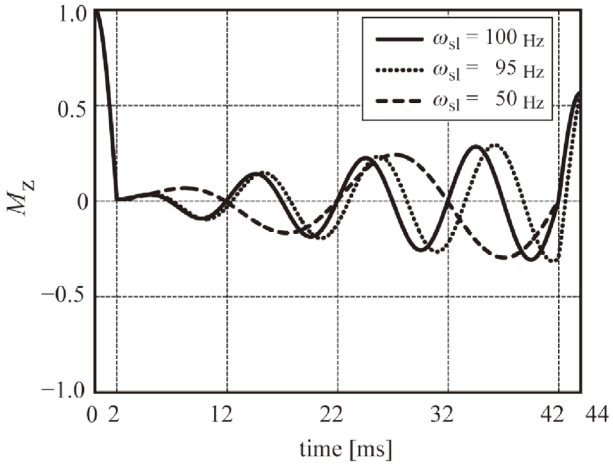

Fig. 5 Time course of M_z. The resonant frequencies were 100, 95, and 50 Hz.

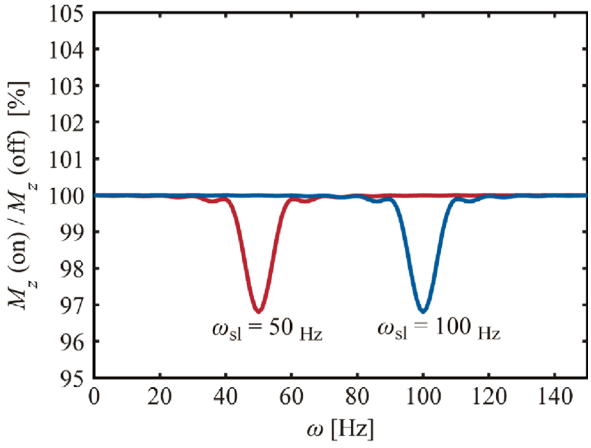

Fig. 6 Normalized magnetization M_z (on) /M_z (off) when ω_{sl} was 50 and 100 Hz while changing ω.

normalized signal intensities, the normalized magnetizations M (on)/M (off) that were obtained from simulations are shown in **Fig. 8** (broken lines). The same tendencies were observed from simulations and phantom studies. However, the phantom studies showed approximately 40% and 70% decreases in normalized signal intensities, while simulations showed approximately 40% decrease in normalized magnetization when ω_{sl} were 50 and 100 Hz, respectively. This difference is probably caused by the difference between the M_z (on) /M_z (off) obtained in simulations and S (on) /S (off) measured in phantoms. The signal intensities observed in measurements were proportional to M_z at the end of the spin-lock module, whereas the signal intensities were influenced by the spin-echo sequence after the spin-lock module. Moreover, the ω giving the maximum S (on)/S (off) decrease was a few Hz lower than ω_{sl}. Magnetic fields oscillating at ω of 41 and 92 Hz decreased S (on) /S (off) to the greatest extent when ω_{sl} was 50 and 100 Hz, respectively.

The phantom studies demonstrated the effect of sub-nT magnetic fields on the intensity of MR signal. Taking into account the results obtained from **Fig. 8**, a magnetic field oscillating at 92 Hz was chosen as the on-resonant oscillating magnetic field expected to give the greatest signal decrease. Ten MR images were acquired in each case: with and without on-resonant oscillating magnetic

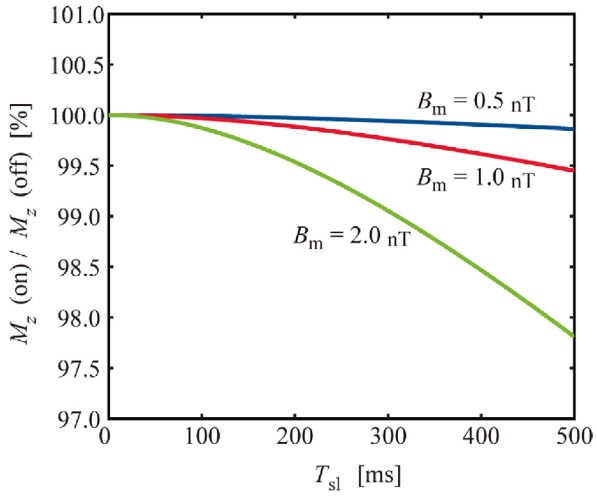

Fig. 7 Normalized magnetization M_z (on)/M_z (off) when B_m were set at 0.5, 1.0, and 2.0 nT while changing T_{sl}.

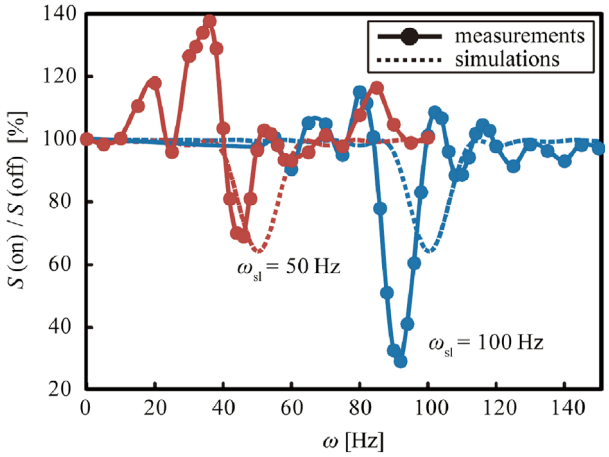

Fig. 8 Normalized signal intensities S (on)/S (off) with ω_{sl} of 50 and 100 Hz while changing ω.

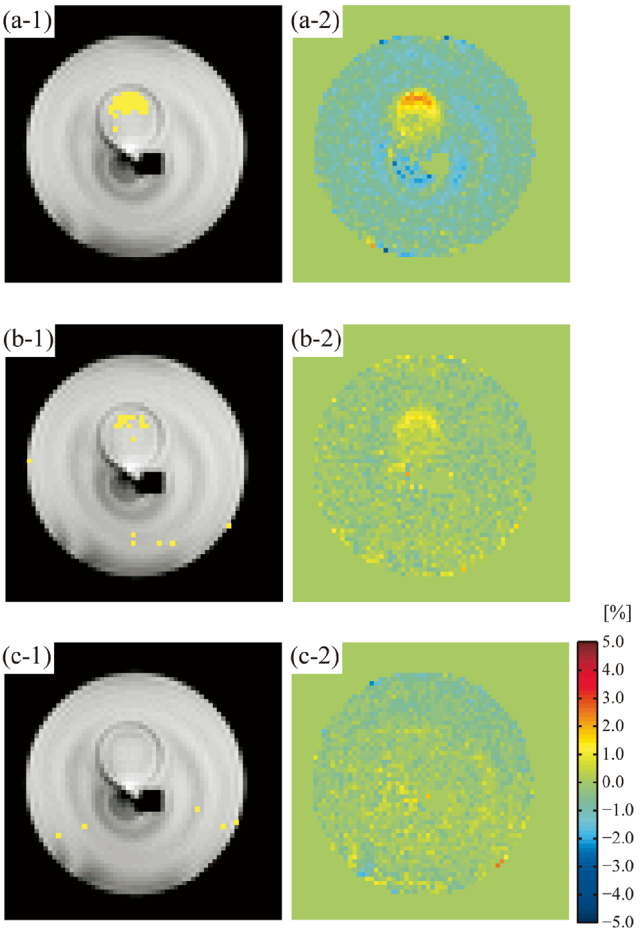

Fig. 9 (Left column) MR images with pixels indicating significant differences. (Right column) Percent signal differences between MR images with and without on-resonant oscillating magnetic fields. The amplitudes of oscillating magnetic field (B_m) are 314 (a), 157 (b) and 31.4 (c) pT.

fields. **Figures 9a-1, b-1, and c-1** show the MR images and pixels (yellow) that show significant differences (two-sided t-tested: $p < 0.05$) in normalized signal intensity between the presence and absence of on-resonant oscillating magnetic fields. **Figures 9a-2, b-2, and c-2** show the percent signal differences between MR images with and without on-resonant oscillating magnetic fields. B_m was 314 (a), 157 (b), and 31.4 (c) pT at the center of the loop. These results demonstrate that acquiring images 10 times allowed the detection of sub-nT magnetic fields.

5. Discussion

Several previous studies have attempted to detect neural magnetic fields using MRI, cell cultures, and theoretical calculations [5–11, 22]. Most of these approached the problem by attempting to observe changes in magnitude or phase images; however, this strategy has the disadvantages of cancellation effects caused by spatially disordered structures, oscillation with a mean phase change of zero, incoherent signals, and location of the current source within the given image voxel [7, 12, 13].

In contrast to this approach, spin-lock imaging potentially detects such signals without cancellation in magnitude or phase images. Spin-lock imaging provides $T_{1\rho}$-weighted images that have previously been achieved in biomedical imaging [18, 23], and has the advantage of allowing band-selective variant experiments such as those shown in **Figs. 6 and 8**. Spin-lock imaging would be of great use in measuring biological sources with multiple consistent frequencies [13]. Witzel et al. [12] and Halpern-Manners et al. [13] proposed an approach of fMRI using the spin-lock imaging sequence based on the secondary magnetic resonance. However, neither research group explained the mechanism of the secondary magnetic resonance in detail. Moreover, the mechanism of fMRI using spin-lock imaging sequence is controversial because the results of fMRI may be contributed by another component, as stated in the study by Jin and Kim [16]. Therefore, in our study we visualized the phenomenon

with numerical Bloch simulations to help understand this approach and investigated how to observe the contributions of externally applied magnetic fields to MR images.

To use spin-lock imaging for fMRI, it must be sufficiently sensitive to neural magnetic fields. Although the possibility of detecting such fields is still a matter of debate, some studies have reported measuring sub-nT magnetic fields using various methods [6, 9, 12, 13]. MEG measurements suggest that evoked or spontaneously synchronized activities in 50,000 or more cortical neurons occupying an area of 1 or a few mm^2 results in magnetic fields of the order of 0.1–1 pT at a distance of 2–4 cm from the neuronal source. In contrast, MRI focusing on voxels 2–4 mm from the site of activation equates to fields in the order of 0.1–1 nT (based on an inverse-square distance scale $(r_{MEG}/r_{MRI})^2$) [9]. It is thus essential to be able to detect magnetic fields of 0.1–1 nT in order to measure brain activation with MRI.

In this regard, we used oscillating magnetic fields with B_m of 0.5, 1.0, and 2.0 nT to detect T_{sl} dependence of M_z (on)/M_z (off) in the Bloch simulation. Employing a longer T_{sl} decreases M_z (on)/M_z (off) to a greater extent, and longer T_{sl} is therefore preferable for observing minute magnetic fields with this method. However, the magnetization decrease is less than 1% when B_m is 0.5 and 1.0 nT, even when we use the longest T_{sl} of 500 ms. This implies that for the fMRI experiments, improvement of the signal-to-noise ratio is necessary, i.e., by increasing the number of repetitive measurements or reducing the noise. Moreover, in attempts to avoid other possible problems of BOLD contamination and susceptibility artifacts, ultra-low-field (ULF) MRI has attracted attention because ULF-MRI virtually cancels these out [15, 24].

Another parameter of the spin-lock pulse; B_{sl}: B_{sl}, affects $T_{1\rho}$ [18, 20]. Like T_1 and T_2^*, $T_{1\rho}$ depends on the magnitude of the static magnetic field B_0, the properties of tissues, and the amplitude of the applied spin-lock pulse (this phenomenon is called $T_{1\rho}$ dispersion) [18]. As a result, measurements of $T_{1\rho}$ based on specific imaging conditions are necessary during simulation.

In the phantom study, we observed decreases in MR signal intensity caused by the secondary magnetic resonance, using magnetic fields oscillating at on-resonant frequencies. However, as shown in **Fig. 8**, there were differences of a few Hz between ω_{sl} and ω that gave maximum decreases in MR signal intensity, and ω_{sl} values were a few Hz lower than expected. This may indicate that B_{sl} values were slightly smaller than the values fixed on the console, which may have been caused by deterioration of the RF coil. Therefore, RF coils capable to output magnetic fields at the correct amplitude should be used.

We also achieved detection of small sub-nT magnetic fields similar in magnitude to neural magnetic fields. When MR images with B_m of 314 and 157 pT at the center of the loop were acquired with and without on-resonant oscillating magnetic fields, significant signal changes were detected. At B_m of 314 pT, as shown in **Fig. 9a-1**, some pixels indicating significant differences between MR images with and without on-resonant oscillating magnetic fields were observed inside the loop. As shown in **Fig. 9a-2**, 1.21% signal changes were observed approximately 2.5 mm from the wire of the loop. The amplitude of magnetization at the pixel given by the Biot-Savart law was 330.4 pT. In addition, as shown in **Figs. 9b-1 and b-2**, 1.49% signal changes were observed approximately 1.25 mm from the wire inside the loop. The amplitude of magnetization was 198.6 pT. Halpern-Manners et al. [13] observed MR images of a single loop at very low driving voltages with estimated field strengths at the center of the loop of 0.92 and 0.46 nT. Furthermore, Witzel et al. [12] reported that a 7 min block design experiment was sensitive to a current dipole that produced an approximate magnetic field of 1 nT at a distance of 1.5 mm from the dipole. In our experiment, the signal-to-noise ratio (SNR) calculated from the average signal and the rms noise in the ROI of acquired MR images without oscillating magnetic fields was 14.9 (ω_{sl} = 50 Hz) and 30.1 (ω_{sl} = 100 Hz). The SNR may be much higher than that of the study by Witzel et al. [12] because of the difference in B_0. Moreover, compared with the study by Halpern-Manners et al. [13] (2.0 and 2.5), the SNR in the present study was much better probably because we employed larger voxel sizes. Therefore, higher SNR in our study may have contributed to the detection of magnetic fields with much lower amplitudes than those in previous studies.

6. Conclusion

In this paper, we described our results of visualizing magnetization behavior based on Bloch simulation to aid understanding of the mechanism of the secondary magnetic resonance during a spin-lock module. We also demonstrated that the secondary magnetic resonance causes remarkable decreases in M_z with externally applied on-resonant oscillating magnetic fields, leading to decreases in MR signal intensity. The results of phantom studies support these findings.

Moreover, in the simulations, we demonstrated that a longer duration of the spin-lock pulse is preferable to accentuate the decrease in MR signal intensity. We therefore selected the duration of 200 ms, which is longer than that used in previous studies [12, 13], but sufficiently short for practical use, and acquired MR image 10 times so as to detect sub-nT magnetic fields. Consequently, we were able to detect magnetic fields of 198.6 pT originated from the single-loop coil. However, for practical fMRI measurements of the human brain, some aspects could be improved, e.g., avoiding contamination of BOLD signals and shortening the acquisition time. To solve these problems, we would like to focus on employing ULF-MRIs or imaging methods that take into account the difference in timescale between the origination of neural magnetic fields and the BOLD effect.

Acknowledgement

The authors thank Dr. Ito, Dr. Imai, and Dr. Takayama for their assistance and discussions. This work was partially

supported by a Grant-in-Aid for Challenging Exploration Research (24650221), a Grant-in-Aid for Scientific Research (A) (24240081), and a Grant-in-Aid for JSPS Fellows (No. 023·5348), all from the Ministry of Education, Culture, Sports, Science, and Technology (MEXT), Japan.

References

1. Ogawa S, Lee TM, Kay AR, Tank DW: Brain magnetic resonance imaging with contrast dependent on blood oxygenation. Proc Natl Acad Sci. **87**(24), pp. 9868–9872, 1990.
2. Arthurs OJ, Boniface S: How well do we understand the neural origins of the fMRI BOLD signal? Trends Neurosci. **25**(1), pp. 27–31, 2002.
3. Höfner N, Albrecht H, Cassará A, Curio G, Hartwig S, Haueisen J, et al.: Are brain currents detectable by means of low-field NMR? A phantom study. Magn Resonance Imaging. **29**(10), pp. 1365–1373, 2011.
4. Turner R: How much cortex can a vein drain? Downstream dilution of activation-related cerebral blood oxygenation changes. NeuroImage. **16**(4), pp. 1062–1067, 2002.
5. Bodurka J, Jesmanowicz A, Hyde J, Xu H, Estkowski L, Li, S J: Current-induced magnetic resonance phase imaging. J Magn Resonance. **137**(1), pp. 265–271, 1999.
6. Bodurka J, Bandettini P: Toward direct mapping of neuronal activity: MRI detection of ultraweak, transient magnetic field changes. Magn Resonance Med. **47**(6), pp. 1052–1058, 2002.
7. Konn D, Gowland P, Bowtell R: MRI detection of weak magnetic fields due to an extended current dipole in a conducting sphere: a model for direct detection of neuronal currents in the brain. Magn Resonance Med. **50**(1), pp. 40–49, 2003.
8. Konn D, Leach S, Gowland P, Bowtell R: Initial attempts at directly detecting alpha wave activity in the brain using MRI. Magn Resonance Imaging. **22** (10), pp. 1413–1427, 2004.
9. Petridou N, Plenz D, Silva AC, Loew M, Bodurka J, Bandettini PA: Direct magnetic resonance detection of neuronal electrical activity. Proc Natl Acad Sci. **103**(43), pp. 16015–16020, 2006.
10. Jay WI, Wijesinghe RS, Dolasinski BD, Roth BJ: Is it possible to detect dendrite currents using presently available magnetic resonance imaging techniques? Med Biol Eng Comput. **50**(7), pp. 651–657, 2012.
11. Park TS, Lee SY: Effects of neuronal magnetic fields on MRI: numerical analysis with axon and dendrite models. NeuroImage. **35**(2), pp. 531–538, 2007.
12. Witzel T, Lin F, Rosen B, Wald L: Stimulus-induced Rotary Saturation (SIRS): A potential method for the detection of neuronal currents with MRI. NeuroImage. **42**(4), pp. 1357–1365, 2008.
13. Halpern-Manners NW, Bajaj VS, Teisseyre TZ, Pines A: Magnetic resonance imaging of oscillating electrical currents. Proc Natl Acad Sci USA. **107** (19), pp. 8519–8524, 2010.
14. Canolty R, Edwards E, Dalal S, Soltani M, Nagarajan S, Kirsch H, et al.: High gamma power is phase-locked to theta oscillations in human neocortex. Science. **313**(5793), pp. 1626–1628, 2006.
15. Kraus Jr RH, Volegov P, Matlachov A, Espy M: Toward direct neural current imaging by resonant mechanisms at ultra-low field. NeuroImage. **39**(1), pp. 310–317, 2008.
16. Jin T, Kim S-G: Characterization of non-hemodynamic functional signal measured by spin-lock fMRI. NeuroImage. **78**, pp. 385–395, 2013.
17. Murase K, Tanki N: Numerical solutions to the time-dependent Bloch equations revisited. Magn Resonance Imaging. **29**(1), pp. 126–131, 2011.
18. Charagundla SR: T1ρ-weighted magnetic resonance imaging: Principles and diagnostic application. Appl Radiol. **33**(1), pp. 32–43, 2004.
19. Wheaton AJ, Borthakur A, Charagundla SR, Reddy R: Pulse sequence for multislice T1ρ-weighted MRI. Magn Resonance Med. **51**(2), pp. 362–369, 2004.
20. Borthakur A, Wheaton A: In vivo measurement of T1ρdispersion in the human brain at 1.5 tesla. J Magn Resonance Imaging. **19**(4), pp. 403–409, 2004.
21. Rooney WD, Johnson G, Li X, Cohen ER, Kim SG, Ugurbil K, et al.: Magnetic field and tissue dependencies of human brain longitudinal 1H2O relaxation in vivo. Magn Resonance Med. **57**(2), pp. 308–318, 2007.
22. Bandettini P, Petridou N, Bodurka J: Direct detection of neuronal activity with MRI: fantasy, possibility, or reality? Appl Magn Resonance. **29**(1), pp. 65–88, 2005.
23. Borthakur A, Hulvershorn J, Gualtieri E, Wheaton AJ, Charagundla S, Elliott MA, et al. : A pulse sequence for rapid in vivo spin-locked MRI. J Magn Resonance Imaging. **23**(4), pp. 591–596, 2006.
24. Cassará A, Maraviglia B, Hartwig S: Neuronal current detection with low-field magnetic resonance: simulations and methods. Magn Resonance Imaging. **27** (8), pp. 1131–1139, 2009.

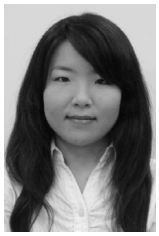

Shizue NAGAHARA

Shizue NAGAHARA received the B.E. and M.E. degrees from Kyoto University, Kyoto, Japan, in 2009 and 2011, respectively. She was trained in medical imaging at School of Medicine, Johns Hopkins University, USA, from 2011 to 2012. Since April 2011, she is a doctoral course student in the Department of Electrical Engineering, Graduate School of Engineering, Kyoto University and is a research fellow of Japan Society for the Promotion of Science (JSPS). Her research interests include functional neuroimaging and magnetic resonance imaging. She is a member of Japanese Society for Magnetic Resonance in Medicine (JSMRM).

Masahito UENO

Masahito UENO received the B.E. degree from Kyoto University, Kyoto, Japan, in 2013. From 2013, he is a master course student in the Department of Electrical Engineering, Graduate School of Engineering, Kyoto University. His research interests include functional neuroimaging and magnetic resonance imaging. He is a member of Japan Biomagnetism and Bioelectromagnetics Society.

Tetsuo KOBAYASHI

Tetsuo KOBAYASHI received his B.S, M.S, and Ph.D. degrees from Hokkaido University, Sapporo, Japan in 1979, 1981 and 1984, respectively. From 2004, he is a professor of the department of electrical engineering, Kyoto University, Kyoto, Japan. His research interests include functional neuroimaging, cognitive neuroscience, optically-pumped atomic magnetometer and ultra-low field MRI. He is a councilor of Institute of Complex Medical Engineering and Japanese Society for Electromagnetic Topography (JSBET). He is also a member of IEEE and Organization for Human Brain Mapping (OHBM).